MULTI-CELL LINEAR PRECODERS FOR MASSIVE MIMO WITH MATRIX NORMALIZATION

Eze Gerald Chukwudi

ABSTRACT
Massive multiple-input multiple-output (mMIMO) is one of the major key enabling technology for future generation networks, which has large number of antennas at both base stations (BSs) and the user equipments (UEs) to provide high throughput using signal processing techniques. In this research work, we studied downlink (DL) sum throughput of mMIMO networks using multi-cell basic linear precoding techniques. The multi-cell zero-forcing (M-ZF), multi-cell regularized zero-forcing (M-RZF), single-cell minimum mean squared error (S-MMSE), and multi-cell minimum mean squared error (M-MMSE) precoding techniques are utilized in the DL. The closed bound expressions of spectrum efficiency (SE) of these linear precoders were derived and analytically expressed. Monte-Carlo simulations were performed with channel-estimators such as minimum mean squared error (MMSE) and element-wise MMSE (EW-MMSE) estimates. The numerical analysis shows that the M-MMSE tends to out-perform S-MMSE, M- RZF, and M-ZF by having the highest average sum throughput at any number of antennas with different UEs in the two-channel estimators. Finally, there is an average sum throughput performance gain of using the M-MMSE over other basic linear precoding techniques.

Keywords: mMIMO, throughput, M-MMSE, S-MMSE, M-RZF, M-ZF.

1 INTRODUCTION

The global demand for frequency spectrum in the wireless access technology has motivated the research and exploration of wireless communication sector known as massive multiple-input multiple-output (mMIMO). Massive MIMO is one of the key enabling technologies for next-generation networks, multiple antenna technology where multiple antennas exist at both the transmitter and receiver. Multiple antennas are equipped at both the base station (BS) and user equipment (UE) or mobile station to boost the transmission and/or reception of communication networks [1]. MIMO technology was categorized into three logical classes viz.: single-user MIMO network, multi-user MIMO network, and massive MIMO network. The massive MIMO Networks are an extended MIMO technology that was introduced in the third generation (3G) technology like LTE/LTE-A, IEEE 802.16e (WiMAX), IEEE 802.11ac/n (WiFi), and other protocols and networks [2]. The massive MIMO involves a massive number of antennas located at the BS and to serve many UEs (or user terminals) at the same time with limited bandwidth and power in cellular communication [3], [4]. Figure 1 depicts a massive MIMO single-cell scenario to serve one or a few users simultaneously; massive MIMO has the following benefits: spectral efficiency (SE), energy efficiency, reliability, and signal processing [6]. The limitations of a massive MIMO network are pilot contamination, channel estimation, radio propagation, and orthogonality of channel responses. In existing literature, factors that affect SE in massive MIMO network are pilot contamination, transmit powers, spatial channel correlation, and pilot reuse factor [7], [8].

The massive MIMO is defined as a network that consists of: (*i*) a number of BS antennas M in the cell that must be far greater than the active number of UE (or mobile terminals) K ($M \gg K$) with antenna-UE ratio $\frac{M}{K} > 1$ in order to achieve effective channel hardening; (*ii*) the number of cells L must be greater than one ($L \geq 2$) working under synchronous time division duplex (TDD) operations/protocol; (*iii*) the transmit precoding and receive linear combining signal processing techniques; and (*iv*) the utilization of BS antennas M with fully digitized transceiver chains and spatially multiplexed number of UE, $K \geq 8$ per single cell [7-8].

• *Eze Gerald Chukwudi is currently pursuing PhD degree program(communication specialization) in electronic engineering in University of Nigeria, Nsukka and a lecturer at Federal Polytechnic Oko, Anambra State, Nigeria. E-mail: eze.gerald@federalpolyoko.edu.ng*

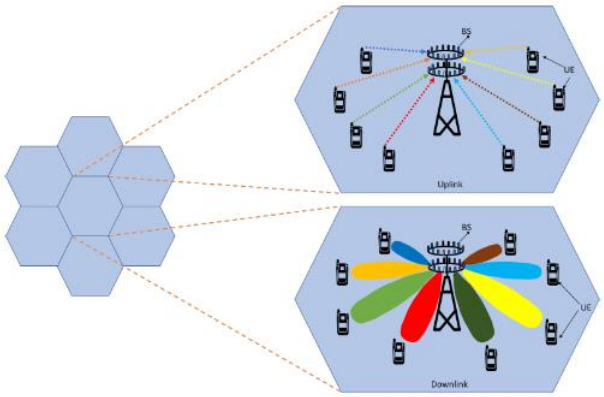

Fig. 1: Massive MIMO network in a cell [1].

There is a massive demand of data traffic in massive MIMO networks within the same scarce bandwidth resources; the number of antennas at BS requires to be raised to serve several UEs at the same time. Therefore, massive MIMO technology has become

leverage for the next generation of wireless communication systems. Massive MIMO has a data throughput of 10–100 times the existing traditional MIMO technology [1]. The MIMO network with a limited number of antennas at BS is already functional, but these small numbers of antennas do not enhance the performance of the network significantly. The sum spectrum efficiency (SE) and data throughput can be boosted remarkably by increasing the number of antennas at BS [7]. Multiple antennas at BS can transmit more data signals to UEs and can separate spatial directed signals by spatial processing techniques [8]. Equipping BS with multiple antennas is more beneficial in SE and data throughput than at mobile UEs. Each addition of antenna at the BS also needs more directivity and transmit power, and this results to more causes complexity in the numerical computation and simulation.

Moreover, the excess of BS antennas increases the SE per UE, allowing high data throughput per UE with high probability. The coherent processing requires accurate channel estimation, which can be obtained through the transmission of known pilot signals. Implementing a TDD protocol enables channel estimates obtained from uplink pilots to be used both for uplink receive combining and DL precoding by utilizing the reciprocity of propagation channels. This makes it possible to operate mMIMO networks with any number of BS antennas. In a multi-cell environment, the reuse of pilot signals between cells causes pilot contamination that decreases the quality of channel estimation and generates coherent interference from/to the pilot-sharing UEs.

In massive MIMO networks, the channel gain becomes more concentrated around its mean when increasing the number of BS antennas. This phenomenon, where a fading channel behaves more deterministically, is called channel hardening. A commonly used model in the performance analysis of massive MIMO is the i.i.d. model, where the UE channels become orthogonal as the number of BS antennas increases. This mutual orthogonality is sometimes referred to as "favorable propagation" [1], [2], [5-8]. Channel hardening and favorable propagation are properties of massive MIMO channels.

Precoding, a downlink signal processing technique is carried out at the base station before the transmission of the signal whereas the uplink signal processing technique is known as decoding [7], [8].

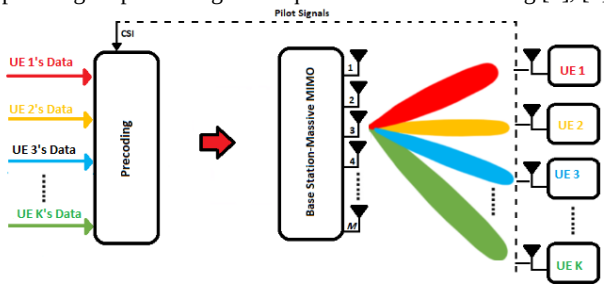

Fig. 2a: Precoding model of massive MIMO networks with M-transmitted base station antennas and K-received single-antenna UE terminals [14].

Data signal from all BS antennas is transmitted to UEs with different amplitude and phases to beam and focus the signal spatially as depicted figure 2a. This is referred to as beamforming but this does not mean that a signal beam is always produced from a particular angular direction and that analog phase-shifters are utilized [8], [13]. In contrast, precoding means that each antenna transmit data signal is produced separately in the digital baseband. This signal has full flexibility in the signal being generated. The downlink signal processing technique referred to as precoding is very pertinent to mitigate the interference between the UEs.

The mMIMO precoding techniques are classified into linear precoding methods, non-linear precoding methods, PAPR precoding methods, and machine-learning-based precoders [14-15].
Linear precoding techniques include [14-15]:

i. Approximate matrix inversion precoders depends mainly on the matrix inversion of the downlink mMIMO channels (examples are truncated polynomial expansion (TPE) algorithm, the Neumann series approximation (NSA) algorithm, the Newton iteration (NI) algorithm, and the Chebyshev iteration (CI) algorithm).
ii. The fixed-point iteration-based linear precoding techniques use iterative algorithm to realize the downlink mMIMO channels (e.g. Gauss-Seidel (GS) algorithm, the successive over-relaxation (SOR) algorithm, the conjugate gradient (CG) algorithm, and the Jacobi iteration (JI) algorithm).
iii. The matrix decomposition based-linear precoding techniques for massive MIMO networks are traditionally used for the matrix inversion process instead of using an explicit matrix inversion in small-scale MIMO networks and it is numerically stable over the basic linear precoder techniques. The matrix decomposition is classified into QR decomposition algorithm and the Cholesky decomposition (CD) algorithms.
iv. The basic linear precoding techniques (or schemes) depend majorly on using the information signals from the BS and the precoding matrix to generate the transmitted signals the UEs. The basic linear precoding techniques are maximum ratio (MR), zero-forcing (ZF), regularized zero-forcing (RZF), single-cell minimum mean squared error (S-MMSE), and multi-cell minimum mean squared error (M-MMSE).

Although linear precoding techniques deteriorate in performance than the other mMIMO precoding techniques under certain scenarios, they still play a vital role in the BS design due to their relative non complexity [14]. The main focus of this work is to investigate multi-cell basic linear precoding techniques in massive MIMO networks for multi-cell scenarios.

A basic linear precoding technique that cancels all the pilot contamination (or interference), both intra-symbol and intra-user interference is the Zero-forcing (ZF) [16], [17]. Zero-forcing (ZF) is the matrix inversion, which produces the desired interference suppression [16].

A regularized form of ZF precoding known as regularized zero-forcing (RZF) is situated between maximum ratio (MR) and zero-forcing (ZF). RZF is sharing the same properties and characteristics with both [16].

A practical remedy for the channel matrix inversion is RZF [7-8], which uses a regularization parameter to make the channel matrix well-posed for the right inversion. Unlike ZF, multiuser interference cannot be cancelled by RZF and thus needs to be appropriately managed by optimizing the regularization parameter. So far, most of the existing works considered the problem of optimizing the

regularization parameter based on the equal-power allocation to UEs, for which the regularization parameter is analytically found for the case of sum SE under sum power constraint, providing that both number of transmit antennas and number of served UEs go to infinity with fixed ratio [20]. This value of the regularization parameter is used for analyzing the SE of RZF [20] or comparing the performance of RZF with that of other techniques [20].

L. D. Nguyen et al. [20] compared the performance achieved by the proposed Multi-user RZF joint design with that achieved by the existing RZF techniques to show the importance of the joint optimization in power allocation and regularization parameter.

Arguably, the most successful and practically applicable precoding scheme used today is RZF precoding [27] also known as minimum mean square error (MMSE) precoding, transmit Wiener filter, generalized eigenvalue-based beamformer, etc.; see [26, Remark 3.2]. Classical RZF precoders are only defined for single cell systems and thus do not take inter-cell interference into account. Disregarding available information about inter-cell interference is particularly detrimental in high density scenarios, where interference is a main performance limiting factor [25]. Multi-cell RZF (M-RZF) is referred to as interference-aware RZF (iaRZF) in [25].

The single-cell minimum mean squared error (S-MMSE) precoding technique amplifies the desired signal but also suppresses coherent and non-coherent interference from within the cell. The single-cell precoding techniques are RZF, ZF, and MR [7-8].

In contrast to S-MMSE, multi-cell minimum mean squared error (M-MMSE) is a multi-cell precoding technique that not only maximizes the desired signal but also suppresses coherent and non-coherent inter-cell and intra-cell interference from the other cells [7-8].

To depict clearly the advantages of M-MMSE technique [18-19], simulation results for M-RZF and M-ZF techniques from [21], and the S-MMSE technique will be provided for comparison in this work using matrix normalization.

2 SYSTEM MODEL

We consider the downlink of a massive MIMO cellular network with multi-cell network up to 16 cells.

The BS of each cell has M antennas and serves K single-antenna UEs in the same time-frequency resource using synchronous time-division duplex (TDD) protocol.

The system model for downlink (DL) may be determined as given in [15]:

$$\boldsymbol{y_{jk}} = \sum_{\boldsymbol{j=1}}^{\boldsymbol{L}} \left(\boldsymbol{h_{jk}}^{\boldsymbol{j}}\right)^{\boldsymbol{H}} \boldsymbol{s_j} + \boldsymbol{n_{jk}} \quad (1)$$

L indicates the number of cells, $\boldsymbol{(.)^H}$ indicates the Hermitian transpose matrix operator and the received DL signal $\boldsymbol{y_{jk}} \boldsymbol{\epsilon}\, \mathbb{C}^{\boldsymbol{M\times K}}$ at UE k in cell j is modeled above. $\boldsymbol{h_{jk}}^{\boldsymbol{j}} \boldsymbol{\epsilon}\, \mathbb{C}^{\boldsymbol{M\times K}}$ is the mMIMO DL channel matrix, where $\mathbb{C}$ denotes a complex value matrix, $\boldsymbol{M}$ is the number of BS antennas represents the number of rows in the matrix and $\boldsymbol{K}$ is the number of UEs represents the number of columns in the matrix, *j* superscript denotes the BS's cell index and *jk* subscripts denote kth UE in cell j.

$$\boldsymbol{h_{jk}}^{\boldsymbol{j}} = \boldsymbol{N_C}\left(\boldsymbol{0}, \boldsymbol{R_{jk}^j}\right) \quad (2)$$

$\boldsymbol{h_{jk}}^{\boldsymbol{j}}$ is the correlated Rayleigh channel and $\boldsymbol{R_{jk}^j} \boldsymbol{\epsilon}\, \mathbb{C}^{\boldsymbol{M\times M}}$ is the spatial correlation matrix, where *j* superscript represents the BS's cell index and *jk* subscripts represent kth UE in cell j. $\boldsymbol{h_{jk}}^{\boldsymbol{j}}$ is modeled by circularly symmetric complex Gaussian distribution having circular symmetry $\boldsymbol{N_C}$ with zero mean and the spatial correlation matrix. The receiver noise may be expressed as

$$\boldsymbol{n_{jk}} = \left(\boldsymbol{0}, \boldsymbol{\sigma^2}\right) \quad (3)$$

Where $\boldsymbol{n_{jk}}$ represents the additive white Gaussian noise (AWGN) vector and $\boldsymbol{s_j}$ is the DL transmit signal [15-16].

2.1 Downlink Channel Estimators

For efficient usage of BS antennas, each BS is required to acquire knowledge of the channels from the UEs which are active in the coherence block [17]. The BS j estimates the channels knowledge from its UEs in a particular cell j. The channel estimates can be determined from the uplink pilot signal $\boldsymbol{Y_j^P}$ received at BS j, which can be defined as [15], [17] expressed in equation (4).

$$\boldsymbol{Y_j^P} = \sum_{\boldsymbol{k=1}}^{\boldsymbol{k_j}} \sqrt{\boldsymbol{p_{jk}}}\, \boldsymbol{h_{jk}}^{\boldsymbol{j}}\, \boldsymbol{\vartheta_{jk}^T} + \sum_{\substack{\boldsymbol{l=1} \\ \boldsymbol{l\neq j}}}^{\boldsymbol{L}} \sum_{\boldsymbol{i=1}}^{\boldsymbol{k_l}} \sqrt{\boldsymbol{p_{li}}}\, \boldsymbol{h_{li}}^{\boldsymbol{j}}\, \boldsymbol{\vartheta_{li}^T} + \boldsymbol{N_j^p} \quad (4)$$

The first part in Equation (4) denotes the desired pilots in the cell, the second part denotes the interfering pilots from other adjacent cells and then the third part $\boldsymbol{N_j^p}$ denotes the receiver noise.

Matrix $\boldsymbol{N_j^p} \boldsymbol{\epsilon}\, \mathbb{C}^{\boldsymbol{M\times \tau_p}}$ contains independent identically distributed elements which follow a complex Gaussian distribution with zero mean and noise variance $\boldsymbol{\sigma^2}$. $\boldsymbol{p_{jk}}$ is deterministic uplink pilot signal and power coefficient for the pilot of user k in cell j. In the channel estimation phase, the aggregated received uplink pilot signals at BS j are denoted as $\boldsymbol{Y_j^P} \boldsymbol{\epsilon}\, \mathbb{C}^{\boldsymbol{M\times \tau_p}}$ where $\boldsymbol{\tau_p}$ is the length of a pilot sequence (and also equals to the number of orthogonal pilot sequences available for the network. Generalized pilot reuse was supported by denoting the relation between $\boldsymbol{\tau_p}$ and $\boldsymbol{K}$ by $\boldsymbol{\tau_p = fK}$, where $\boldsymbol{f}$ is the pilot reuse factor (1, 2, 4 or 16) [17]. The universal pilot reuse factor of *f* =1 and non-universal pilot reuse factors of *f* = 2, 4, 16 [11]. The mutually orthogonal uplink pilot matrix $\boldsymbol{\tau_p}$ was organized as columns at BS j, $\boldsymbol{\vartheta_j = [\vartheta_{j1}, \vartheta_{j2}, \vartheta_{j3}, \dots, \vartheta_{jk}] \epsilon\, \mathbb{C}^{\tau_p \times K}}$ which were transmitted by the kth UE of the cell j. All pilot sequences are assumed to originate from a predefined orthogonal pilot book in which sequence $\boldsymbol{\vartheta_{li}^T} \boldsymbol{\epsilon}\, \mathbb{C}^{\boldsymbol{\tau_p}}$ was defined as below [15] and [17] expressed in equations (5a) to equation (6):

BS j correlates $\boldsymbol{Y_j^P}$ with $\boldsymbol{\vartheta_{jk}^*}$ to estimate $\boldsymbol{y_{jk}}^{\boldsymbol{j}\ \boldsymbol{p}}$.

$$\boldsymbol{y_{jk}}^{\boldsymbol{j}\ \boldsymbol{p}} = \boldsymbol{Y_j^P \vartheta_{jk}^*} \quad (5a)$$

$$\boldsymbol{\vartheta_{jk}}^{\boldsymbol{H}} \boldsymbol{\vartheta_{ik}} = \begin{cases} \boldsymbol{\tau_p} & \boldsymbol{when\ j = i} \\ \boldsymbol{0} & \boldsymbol{when\ j \neq i} \end{cases} \quad (5b)$$

MMSE Channel Estimator may be expressed in equation (6) as obtained in [15] and [17]

$$\widehat{\boldsymbol{h}}_{\boldsymbol{jk}}^{\ \boldsymbol{j}} = \sqrt{\boldsymbol{p_{jk}}}\, \boldsymbol{R_{jk}^j Z_{jk}^j}\, \boldsymbol{y_{jk}}^{\boldsymbol{j}\ \boldsymbol{p}} \quad (6)$$

$$\boldsymbol{Z_{jk}^j} = \left(\sum_{(\boldsymbol{j'},\boldsymbol{k'}) \in \boldsymbol{q}} \boldsymbol{p_{j'k'} \tau_p R_{j'k'}^j} + \boldsymbol{\sigma^2 I_M} \right)^{-1} \quad (7a)$$

$\boldsymbol{R_{jk}^j} \boldsymbol{\epsilon}\, \mathbb{C}^{\boldsymbol{M\times M}}$ is the spatial correlation matrix, where *j* superscript represents the BS's cell index and *jk* subscripts represent kth UE in

cell j. $\boldsymbol{Z_{jk}^{j}}$ is the matrix of the inverse of the normalized processed signal correlation matrix defined in [15].

$$\boldsymbol{q} = \{(j', k') : \vartheta_{jk} = \vartheta_{j'k'},\ j' = 1, 2, 3 \dots j,\ k' = 1, 2, 3 \dots k\} \quad (7b)$$

τ_p samples are reserved for UL pilot signaling in each coherence block. The set above defines the indices of all mobile terminals (UEs) that use the same pilot sequence as user (UE) *j* in cell *k*. Hence, (*j'*, *k'*) ∈ q implies that UE *k'* in cell *j'* uses the same pilot as UE *k* in cell *j*.

EW-MMSE Channel Estimator may be expressed in equation (8) as obtained in [15] and [17]:

$$\left[\hat{\boldsymbol{h}}_{jk}{}^{j}\right]_m = \frac{\sqrt{p_{jk}}\left[\boldsymbol{R}_{jk}^{j}\right]_{mm}}{\sum_{(j',k')\in q} \boldsymbol{p}_{j'k'}\boldsymbol{\tau}_p\left[\boldsymbol{R}_{j'k'}^{j}\right]_{mm} + \boldsymbol{\sigma}^2} \boldsymbol{y}_{jk}^{j\ p} \quad (8)$$

Where $\hat{\boldsymbol{h}}_{jk}{}^{j}$ is the ***EW-MMSE estimate*** of $\boldsymbol{h}_{jk}{}^{j}$**,** [15-17].

The matrices transmit precoding:

The transmit powers of all UEs in jth cell from BS *j:*

$$\boldsymbol{P_J} = \boldsymbol{diag}\left(\boldsymbol{P}_{j1}, \boldsymbol{P}_{j2}, \boldsymbol{P}_{j3} \dots \boldsymbol{P}_{jk}\right) \in \mathbb{C}^{K\times K} \quad (10a)$$

Subscripts of estimated channel matrix $\hat{\boldsymbol{H}}_{jl}$ in Eqn. (10b) below denote the channel connection between BS j and all the UEs in cell l with the MIMO DL channel.

$$\hat{\boldsymbol{H}}_{jl} = \hat{\boldsymbol{h}}_{lk}{}^{j} \quad (10b)$$

2.2 The Multi-cell basic linear precoding techniques

Single-cell minimum mean squared error (S-MMSE) may be expressed in equation (11a) as obtained in [6-7] and [18-19].

$$\boldsymbol{F_J^{S-MMSE}} = \left(\hat{\boldsymbol{H}}_{jj}\boldsymbol{P_J}\left(\hat{\boldsymbol{H}}_{jj}\right)^{\boldsymbol{H}} + \boldsymbol{Z_J}\right)^{-1}\hat{\boldsymbol{H}}_{jj}\boldsymbol{P_J} \quad (11a)$$

$$\boldsymbol{Z_J} = \sum_{i=1}^{K_j}\boldsymbol{p}_{ji}\boldsymbol{C}_{ji}^{j} + \sum_{\substack{l=1\\ l\neq j}}^{L}\sum_{i=1}^{K_l}\boldsymbol{p}_{li}\boldsymbol{R}_{li}^{j} + \boldsymbol{\sigma}^2\boldsymbol{I}_M$$

Multi-cell minimum mean squared error (M-MMSE) may be expressed in equation (11b) as obtained in [6-7] and [18-19].

$$\boldsymbol{F_J^{M-MMSE}} = \left(\sum_{l=1}^{L}\hat{\boldsymbol{H}}_{jl}\boldsymbol{P}_l\left(\hat{\boldsymbol{H}}_{jl}\right)^{\boldsymbol{H}} + \boldsymbol{Z_J}\right)^{-1}\hat{\boldsymbol{H}}_{jj}\boldsymbol{P_J} \quad (11b)$$

$$\boldsymbol{Z_J} = \sum_{l=1}^{L}\sum_{i=1}^{K_l}\boldsymbol{p}_{li}\boldsymbol{C}_{li}^{j} + \boldsymbol{\sigma}^2\boldsymbol{I}_M$$

P_l is transmitting powers of all UEs from BS j in cell *l*.

For MMSE precoding in (11a) and (11b), $\boldsymbol{Z_J}$ has bounded spectral norm while $\hat{\boldsymbol{H}}_{jj}\boldsymbol{P_J}\left(\hat{\boldsymbol{H}}_{jj}\right)^{\boldsymbol{H}}$ has LK eigenvalues that grow unboundedly as M approaches infinity. As the impact of $\boldsymbol{Z_J}$ vanishes, the approach can be used to prove that M-MMSE approaches M-ZF asymptotically.

Multi-cell zero forcing (M-ZF): may be expressed in equation (11c) as obtained in [21] and [22]. Zero forcing (ZF) was the first performance technique to introduce matrix inversion, which is used to suppress or lessen intra-cell interference that is interference from UEs within the same cell.

$$\boldsymbol{F_J^{M-ZF}} = \hat{\boldsymbol{H}}_{jj}\left(\sum_l\left(\hat{\boldsymbol{H}}_{jl}\right)^{\boldsymbol{H}}\hat{\boldsymbol{H}}_{jl}\right)^{-1} \quad (11c)$$

Multi-cell regularized zero forcing (M-RZF): may be expressed in equation (11d) as obtained in [21-22] and [25].

$$\boldsymbol{F_J^{M-RZF}} = \hat{\boldsymbol{H}}_{jj}\boldsymbol{P}_j\left(\sum_l\boldsymbol{P}_j\left(\hat{\boldsymbol{H}}_{jl}\right)^{\boldsymbol{H}}\hat{\boldsymbol{H}}_{jl} + \boldsymbol{\sigma}^2\boldsymbol{I}_K\right)^{-1} \quad (11d)$$

2.3 Precoding and Matrix Normalization (MN) Method

The transmitted signal s_j in equation (1) may be expressed in [15] and [17] as:

$$\boldsymbol{s_j} = \sum_{i=1}^{k_j}\boldsymbol{w}_{ji}\,\boldsymbol{d}_{ji} \quad (12a)$$

The transmitted signal $\boldsymbol{s_j}$ from jth BS antennas M in a cell can consist of multiple information data signals $\boldsymbol{d_{ji}}$ that are transmitted making use of different precoding vector $\boldsymbol{w_{ji}}$ from jth BS (e.g., different spatial directivity). If there are K UEs unit power DL data vector $\boldsymbol{d_{ji}} = [\boldsymbol{d_{j1}}, \dots, \boldsymbol{d_{jK}}]$ from jth BS intended for K different UEs in the cell. The transmitted signal $\boldsymbol{s_j}$ may obtain by the multiplication of the precoding vector $\boldsymbol{w_{ji}}$ and the information DL data vectors $\boldsymbol{d_{ji}}$. The precoding vector $\boldsymbol{w_{ji}}$ determines the direction of the spatial directivity of the DL data signals $\boldsymbol{d_{ji}}$**,** while the squared norm $||\boldsymbol{w_{ji}}||^2$ determines the associated transmit power.

Matrix normalization (MN) technique: In this technique, when we select the any precoding matrix F and all the entries are scaled with the square root of maximum transmit power $\boldsymbol{P}$ which is used to satisfy (12c). More precisely, we express matrix normalization technique as

$$\boldsymbol{W} = \frac{\sqrt{\boldsymbol{P}}}{||\boldsymbol{F}||_{\boldsymbol{F}}}\boldsymbol{F} \quad (12b)$$

The computation of the precoding matrix at BS j requires MK complex multiplications, which are needed to compute $||\boldsymbol{F}||_{\boldsymbol{F}}$ in equation (12b) for all UEs at once [3]. We must ensure that the squared Frobenius norm of $\boldsymbol{W}$ equals the maximum transmit power [1-6]:

$$\boldsymbol{trace}(\boldsymbol{W}\times\boldsymbol{W}^{\boldsymbol{H}}) \leq \boldsymbol{P} \quad (12c)$$

Where precoding matrix $\boldsymbol{W}\in\mathbb{C}^{M\times K}$ is defined as the M×K-dimensional precoding matrix. Massive MIMO usually means that $\frac{\mathbf{M}}{\mathbf{K}} > \mathbf{1}$ and $\mathbf{M}\gg\mathbf{K}$.

2.4 Downlink SINR, Spectral Efficiency (DL SE), and Network throughput:

The expression for the effective downlink SINR as given in [15-17] and [15] is expressed in equation (13).

$$\boldsymbol{SINR_{jk}^{DL}} = \frac{\boldsymbol{p}_{jk}\left|\mathbb{E}\{\boldsymbol{w}_{jk}^{H}\boldsymbol{h}_{jk}{}^{j}\}\right|^2}{\sum_{l=1}^{L}\sum_{i=1}^{K}\boldsymbol{p}_{li}\left|\mathbb{E}\{\boldsymbol{w}_{li}^{H}\boldsymbol{h}_{jk}{}^{l}\}\right|^2 - \boldsymbol{p}_{jk}\left|\mathbb{E}\{\boldsymbol{w}_{jk}^{H}\boldsymbol{h}_{jk}{}^{j}\}\right|^2 + \boldsymbol{\sigma}^2} \quad (13)$$

The expectation $\mathbb{E}\{\}$ is determined with reference to channel realizations. Therefore, a downlink SE maximizes the SINR in Eqn. (14) for a given channel estimates are derived in [15-17]:

$$\boldsymbol{SE_{jk}^{DL}} = \frac{\tau_c-\tau_p}{\tau_c}\boldsymbol{\log_2}\left(\mathbf{1} + \boldsymbol{SINR_{jk}^{DL}}\right) \quad (14)$$

The term $\frac{\tau_c-\tau_p}{\tau_c}$ is the Prelog factor that represents the portion of samples per coherence interval that are used for downlink data transmission. Network throughput (bits/s) value is obtained by the multiplication of operational Bandwidth (Hz) and SE (bits/s/Hz).

$$\boldsymbol{Network\ throughput}\left(\frac{\boldsymbol{bit}}{\boldsymbol{s}}\right) = \boldsymbol{Bandwidth}\ (\boldsymbol{Hz}) \times \boldsymbol{SE_{jk}^{DL}}\left(\frac{\frac{\boldsymbol{bit}}{\boldsymbol{s}}}{\boldsymbol{Hz}}\right) \quad (15)$$

3 SIMULATION RESULTS AND DISCUSSION

There are four methods to generate the channel covariance matrices and the resulting spatial correlation. For an arbitrary user, the

covariance matrix **R** can be modeled by using Local Scattering Spatial Correlation Model with Gaussian distribution, Laplace distribution, Exponential distribution and Uniform angular distribution in [8] and [22]. Fig. 2b illustrates the eigenvalue distribution with the four covariance models for Number of BS antennas, M = 200 antennas, the nominal angle = 30˚and Angular standard deviation = 10˚. The covariance matrices are normalized such that trace (**R**) = M. The aforementioned four distributions of the angular deviations are compared with the reference case of uncorrelated fading below.

.

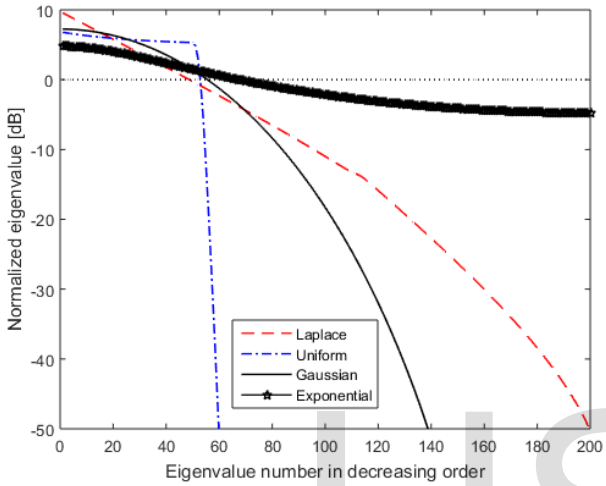

Fig. 2b: Eigenvalues of the spatial covariance matrix **R** when using the local scattering model with M = 200 and uncorrelated fading is shown as a reference case.

All four angular distributions create larger eigenvalue variations, but there are substantial differences. The Uniform angular distribution provides rank-deficient covariance matrices, where a large fraction of the eigenvalues is zero. In contrast, the other three angular distributions provide full-rank covariance matrices with more modest eigenvalue variations. In the remainder, we consider only exponential distribution to emphasize that our main results only require linear independence between the covariance matrices, not rank-deficiency (which in special cases give rise to orthogonal covariance supports [22]). Uncorrelated fading is shown as a reference case where all eigenvalues of covariance matrix are equal.

A square pattern network layout is used in [8]. The 4-cell setup is utilized and each cell has an area of 90 km^2 [22]. Inter-cell and intra-cell interference receive by all the base stations are the same in all directions. The calculate large-scale fading coefficient, was calculated with a channel gain of -35.3 at 1 km, path loss factor of -3.76, and standard deviation of fading value 10. The operating bandwidth of 20 MHz with a noise variance and noise figure 10dB was used. A 100mW downlink transmit power was allocated to each UE in a particular cell and the number of UEs per cell given as 2 and 10 [22]. The UEs were equally distributed in each cell.

The simulation results were produced using the code in [22]. In this section, we will show numerically that an unlimited throughput is achievable under pilot contamination. To this end, the correlation (covariance) matrix R was modeled by Exponential correlation model for a ULA with correlation factor r of 0.5. Exponential correlation model is selected due to full-rank covariance matrices with modest eigenvalue variations than uncorrelated Rayleigh fading with non eigenvalue variations [22].

TABLE 1
SIMULATION PARAMETERS

Parameter	Value
Network layout	Square pattern (wrap-around)
Number of Cells	4
Number of BS antennas	200
Communication Bandwidth	20 MHz
DL transmit power	100mW (-10dB)
Noise Figure	10dB
Noise Variance	$-174 + 10\log_{10} B +$ Noise Figure
Pathloss exponent	3.76
Shadow fading (standard deviation)	10
Distance between BSs	300
Average channel gain using the large-scale fading model	$-35.3 - 37.6\log_{10} d_{lk}^{j}$
Standard deviation of large-scale fading variations	4
Total coherence block length (τ_c)	200
Channel Model	Exponential correlation model
Number of channel realizations per setup	1000
Correlation factor (r)	0.5

Impact on network throughput

Network throughput is one of the vital metric to evaluate network performance in mMIMO networks. This metric is expressed in equation (15) and measures the quality of service (QoS) of the network. In order to examine the impact of throughput on performance, we simulated by increasing the number of antennas in the network, to exemplify the performance of the network. Figures 3, 4, 5, and 6 show the comparison on the network throughput metric. In figures 3 and 4, the exponential correlation model with r = 0.5 is used, but with large-scale fading variations over the array with $\sigma = 4$.

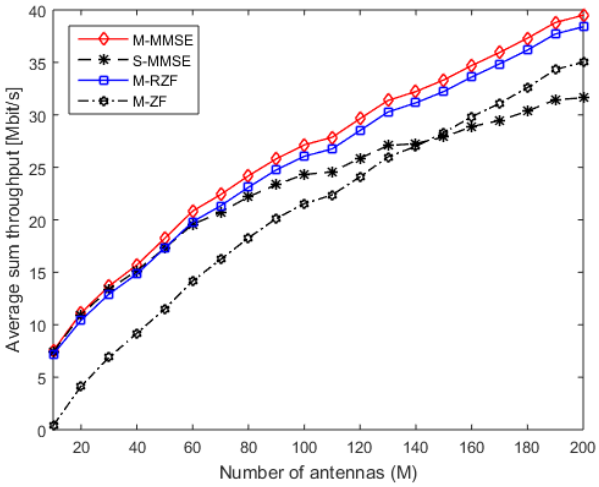

Fig. 3: Downlink throughput as a function of M for K = 2, when using either the MMSE estimator with full covariance knowledge.

M-MMSE and M-RZF precoding are both suboptimal when compared to S-MMSE and M-ZF, but they can be shown to be asymptotically equal in the downlink. Interestingly, the same behaviors are observed in Fig.4 when using the EW-MMSE estimator, which is a suboptimal estimator that neglects the off diagonal elements of the covariance matrices.

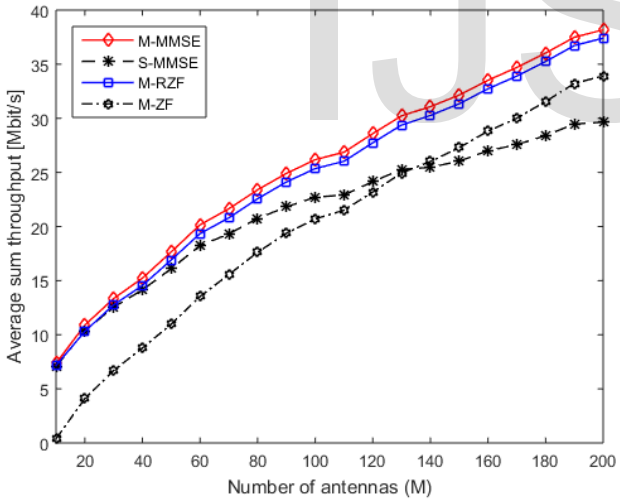

Fig. 4: Downlink throughput as a function of M for K = 2, when using either the EW-MMSE estimator with known diagonals of the covariance matrices.

There is a small throughput loss of 2%–4% for M-MMSE, S-MMSE, M-RZF and M-ZF precoders using EW-MMSE estimator compared to Fig. 3, but this is a minor price to pay for the greatly simplified acquisition of covariance information (estimating the entire diagonal is as simple as estimating a single parameter [23], [24]).

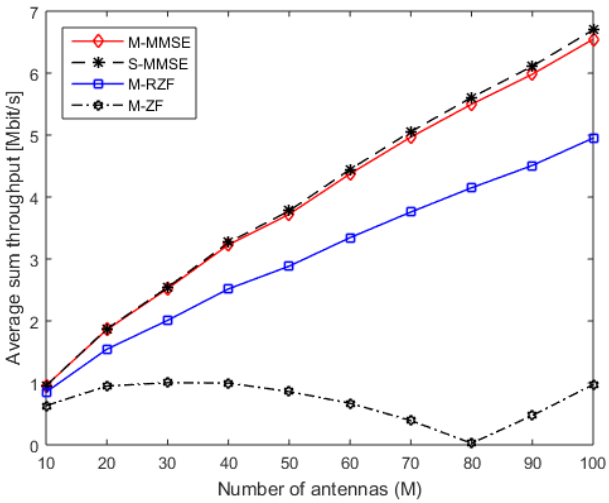

Fig. 5: Downlink SE as a function of M for K = 20 UEs that are uniformly distributed in the shaded cell edge area, when using either the MMSE estimator with full covariance knowledge. .

We now increase the number of UEs per cell to K = 20, which leads to more interference but the same pilot contamination per UE. The UEs are uniformly and independently distributed in the cell-edge area, which is the shaded area in [22, fig. 3]. The channel model is the same as in the previous figures 3 and 4.

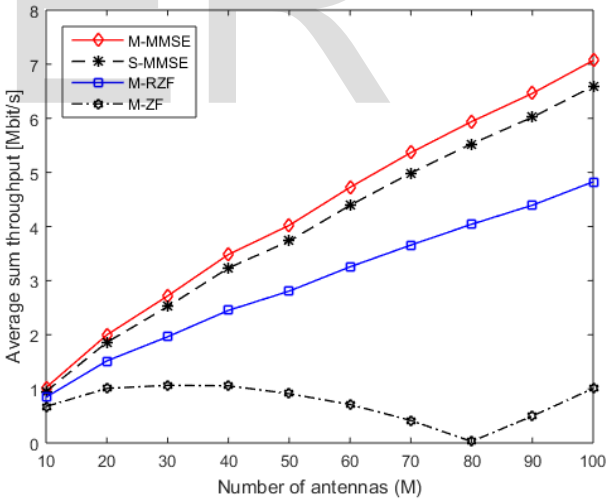

Fig. 6: Downlink throughput as a function of M for K = 20 UEs that are uniformly distributed in the shaded cell edge area, when using the EW-MMSE estimator with known diagonals of the covariance matrices.

The downlink throughput per UE is shown in figures 5 and 6 when using either MMSE or EW-MMSE estimation. The results resemble the ones for K = 2, but the curves are basically shifted to the right due to the additional interference. M-MMSE and S-MMSE provide throughputs that grow without bound, while the throughput with M-RZF and M-ZF saturate, but more antennas are needed before reaching saturation.

4 CONCLUSION

Massive MIMO is a multi-cellular MU-MIMO network that uses a large-scale number of BS antennas to spatially multiplex many UEs in the same time–frequency resource, but with substantially more antennas than UEs to protect against interference. The spatial multiplexing allows a sum throughput that increases almost linearly with the number of BS antennas, which can lead to orders of magnitude increase in sum throughput. The above figures depict throughput performance metrics with multi-cell precoding techniques such as M-MMSE, S-MMSE, M-RZF, and M-ZF. The throughput of the M-RZF and M-ZF are not the same. By adding more antennas at BS and simultaneously serving multiple UEs in multi-cell with the same time-frequency resources, sum throughput is improved significantly. Finally, there is an average sum throughput gain of using M-MMSE over other precoding techniques such as S-MMSE, M-RZF, and M-ZF with low complexity.

ACKNOWLEDGMENT

The author wishes to thank Prof. Ani C. I and Dr. Chidera Anioke of department of electronic engineering in University of Nigeria, Nsukka.

REFERENCES

[1] Robin Chataut and Robert Akl, "Massive MIMO Systems for 5G and beyond Networks—Overview, Recent Trends, Challenges, and Future Research Direction," Sensors 2020, 20, 2753; doi:10.3390/s20102753.

[2] E. Björnson, E. G. Larsson, and T. L. Marzetta, "Massive MIMO: ten myths and one critical question," IEEE Commun. Mag, Vol. 54, no. 2, pp. 114–123, Feb. 2016.

[3] E. Björnson, L. Sanguinetti, H. Wymeersch, J. Hoydis, and T. L. Marzetta, "Massive MIMO is a reality—what is next?: Five promising research directions for antenna arrays," Digital Signal Process., Elsevier, vol. 94, pp. 3–20, June 2019.

[4] Thomas L. Marzetta, "Massive MIMO: An Introduction," Bell Labs Technical Journal, vol. 20, pp.11-22, 2015.

[5] E. Ali, M. Ismail, R. Nordin, and N. F. Abdulah, "Beamforming techniques for massive MIMO systems in 5G: Overview, classification, and trends for future research," Front. Informat. Tech. Elect. Eng., Springer, vol. 18, no. 6, pp. 753–772, June 2017.

[6] J. Kaur, M. L. Singh, and R. S. Sohal, "Analysis of sum spectrum efficiency in multiple antennas multi-user MIMO cellular system for millimeter wave communications," Indian Academy of Sciences, Sådhanå (2019) 44:180, pp. 1-9, Jun. 2019. [Online:] https://doi.org/10.1007/s12046-019-1162-5.

[7] L. Sanguinetti, E. Björnson and J. Hoydis, "Towards Massive MIMO 2.0: Understanding spatial correlation, interference suppression, and pilot contamination," IEEE Transactions on Communications, 0090-6778, 2019. DOI:10.1109/TCOMM.2019.2945792

[8] E. Björnson, J. Hoydis, and L. Sanguinetti, "Massive MIMO Networks: Spectral, Energy, and Hardware Efficiency," Foundations and Trends in Signal Processing, Vol. 11, No. 3-4, pp 154–655, 2017. DOI: 10.1561/2000000093

[9] Dongmei Zhang, Ximing Wang, Kui Xu, Yijun Yang and Wei Xie, "Multiuser 3D massive MIMO transmission in full-duplex cellular system," EURASIP Journal on Wireless Communications and Networking, 2018.

[10] M. Sadeghi, L. Sanguinetti, R. Couillet, and C. Yuen, "Large system analysis of power normalization techniques in Massive MIMO," IEEE Trans. Veh. Technol, Vol. 66, no. 10, pp. 9005–9017, Oct. 2017.

[11] Özgecan Özdogan, "Analysis of Cellular and Cell-Free Massive MIMO with Rician Fading," Linköping Studies in Science and Technology Thesis No. 1870, Div. of Comm. Systems, Dept. Elect. Eng., Linköping Univ., Linköping, Sweden, 2020.

.

[12] J. Singh and D. Kedia "Spectral Efficient Precoding Design for Multi-cell Large MU-MIMO System," IETE Journal of Research, pp. 1–17, Jul. 2020. [Online:] https://doi.org/10.1080/03772063.2020.1791745

[13] Özgecan Özdogan, Emil Björnson, and Erik G. Larsson, "Massive MIMO with Spatially Correlated Rician Fading Channels," IEEE Transactions on Communications, 2019.DOI: 10.1109/TCOMM.2019.2893221

[14] M. A. Albreem, A. Alhabbash, A. M. Abu-Hudrouss, and S. Ikki, "Overview of Precoding Techniques for Massive MIMO," IEEE Access, April 2021. DOI:10.1109/ACCESS.2021.3073325.

[15] M. A. Albreem, M. Juntti, and S. Shahabuddin, "Massive MIMO detection techniques: A survey," IEEE Commun. Surveys Tuts., vol. 21, no. 4, pp. 3109–3132, 2019.

[16] Fa-Long Luo and Charlie (Jianzhong) Zhang, *"*Massive MIMO for 5G: Theory Implementation and Prototyping,*"* in Signal processing for 5G: algorithms and implementations, John Wiley & Sons, Ltd. 2016. *pp. 190-230.*

[17] N. Fatema, G. Hua, Y. Xiang, D. Peng, and I. Natgunanathan, "Massive MIMO linear precoding: A survey," IEEE Syst. J., vol. 12, no. 4, pp.3920–3931, Dec 2018.

[18] X. Li, E. Bjornson, E. G. Larsson, S. Zhou, and J. Wang, "A multicell MMSE precoder for massive MIMO systems and new large system analysis," in IEEE Int. Conf. Global Commun. (GLOBECOM), San Diego, CA, Dec 2015, pp. 1–6.

[19] X. Li, E. Bjornson, E. G. Larsson, S. Zhou, and J. Wang, "Massive MIMO with multi-cell MMSE processing: exploiting all pilots for interference suppression," EURASIP Journal on Wireless Communications and Networking, 2017.

[20] L. D. Nguyen, H. D. Tuan, T. Q. Duong, and H. V. Poor, "Multi-user regularized zero-forcing beamforming," IEEE

Transactions on Signal Processing, 1053-587X (c) 2018 IEEE. DOI 10.1109/TSP.2019.2905833

[21]E Björnson, E G Larsson, M Debbah, "Massive MIMO for maximal spectral efficiency: How many users and pilots should be allocated?" IEEE Trans. Wireless Commun. **15**(2), 1293–1308, 2016.

[22] E. Björnson, J. Hoydis, and L. Sanguinetti, "Massive MIMO has unlimited capacity," IEEE Trans. Wireless Commun, Vol. 17, no. 1, pp. 574–590, Jan. 2018.

[23] N. Shariati, E. Bjornson, M. Bengtsson, and M. Debbah, "Low complexity polynomial channel estimation in large-scale MIMO with arbitrary statistics," IEEE J. Sel. Topics Signal Process., vol. 8, no. 5,pp. 815–830, Oct. 2014.

[24] E. Bjornson, L. Sanguinetti, and M. Debbah, "Massive MIMO with imperfect channel covariance information," in Proc. ASILOMAR, 2016.

[25] A. Muller, R. Couillet, E. Bjornson, S. Wagner, and M. Debbah, "Interference-Aware RZF Precoding for Multi Cell Downlink Systems," IEEE Transactions on Signal Processing, Vol. 63, No. 15, pp. 3959–3973, August, 2015.

[26] E. Bjornson and E. Jorswieck, "Optimal Resource Allocation in Coordinated Multi-Cell Systems," Foundations and Trends in Communications and Information Theory, vol. 9, no. 2-3, pp. 113–381, 2013.

[27] C. Peel, B. Hochwald, and A. Swindlehurst, "A Vector-Perturbation Technique for Near-Capacity Multiantenna Multiuser Communication—Part I: Channel Inversion and Regularization," IEEE Transactions on Communications, vol. 53, no. 1, pp. 195–202, 2005.